



Intracellular delivery of His-tagged proteins via a hybrid organic–inorganic nanoparticle

Haisen Zhou¹ · Yaoyi Wang¹ · Hua Lu¹

Received: 1 May 2021 / Revised: 25 May 2021 / Accepted: 26 May 2021
© The Society of Polymer Science, Japan 2021

Abstract

Intracellular delivery of proteins remains challenging. Here, we present a simple and general platform for the efficient loading and delivery of proteins using a methoxy-poly(ethylene glycol)-*block*-poly(L-phosphotyrosine) (mPEG-*b*-PpY)-templated calcium phosphate (CaP) hybrid nanoparticle. By doping hybrid CaP nanoparticles with Zn²⁺ (CaP-Zn), recombinant proteins bearing a histidine tag can be conveniently loaded by harnessing the His-Zn coordination bond. The resulting protein@CaP-Zn nanoparticles display low toxicity and are tunable, uniform in size, stable under physiological conditions, and degradable in acidic milieu for responsive release. Proteins loaded onto the CaP-Zn nanoparticle can be protected from proteolytic degradation and effectively delivered to intracellular spaces. This work may open up opportunities for protein activity preservation and facilitate the intracellular delivery of recombinant protein therapeutics.

Introduction

Owing to their high bioactivity and specificity, protein-based therapeutics have been successful as one of the fastest growing classes of drugs on the market [1]. It was reported that out of the top ten bestselling drugs globally in 2020, five are protein-based therapeutics [2]. However, because of the inability of most proteins to permeate membranes, all of the current protein drugs on the market have been developed to act on extracellular targets [3]. Moreover, native proteins are prone to proteolytic degradation and renal clearance due to their vulnerable hierarchical structure and small size. Therefore, carrier systems for the efficient intracellular delivery of protein drugs are highly desirable [4–13].

To fulfill this goal, multifunctional and intelligent materials need to be designed that can interact and bind with proteins with suitable affinity, protect proteins from degradation, transport proteins across the cellular membrane, and implement cytosolic cargo release with responsive properties [14]. Unlike nucleotides that are uniformly negatively charged and can simply be condensed via electrostatic forces, proteins are highly diverse in their physicochemical properties [3]. Moreover, the surfaces of proteins are highly heterogeneous in terms of charge distribution, hydrophobicity, and hydrogen bonding pairs [15]. This has raised notable hurdles in the physical encapsulation of proteins via simple noncovalent interactions. The covalent conjugation of proteins to their delivery carriers can solve this problem to some extent, but requires a sophisticated design consisting of degradable linkers and laborious protein modification and product purification efforts [16–18]. Moreover, random labeling of proteins can lead to the inevitable loss of protein activity [19]. Thus, an efficient and general protein binding strategy sparing the efforts of covalent labeling would significantly facilitate the development of protein delivery [20–25].

Histidine tags (His-tags) have been widely used in protein expression and purification. The attachment of a His-tag allows proteins to be easily enriched on a Ni-NTA-based affinity column and thus separated from other components [26, 27]. Harnessing the chelating interaction of His-tags and divalent transition metal ions, various His-tagged synthetic peptides and recombinant proteins have been incorporated

Supplementary information The online version contains supplementary material available at <https://doi.org/10.1038/s41428-021-00526-7>.

✉ Hua Lu
chemhualu@pku.edu.cn

¹ Beijing National Laboratory for Molecular Sciences, Center for Soft Matter Science and Engineering, Key Laboratory of Polymer Chemistry and Physics of Ministry of Education, College of Chemistry and Molecular Engineering, Peking University, Beijing, People's Republic of China

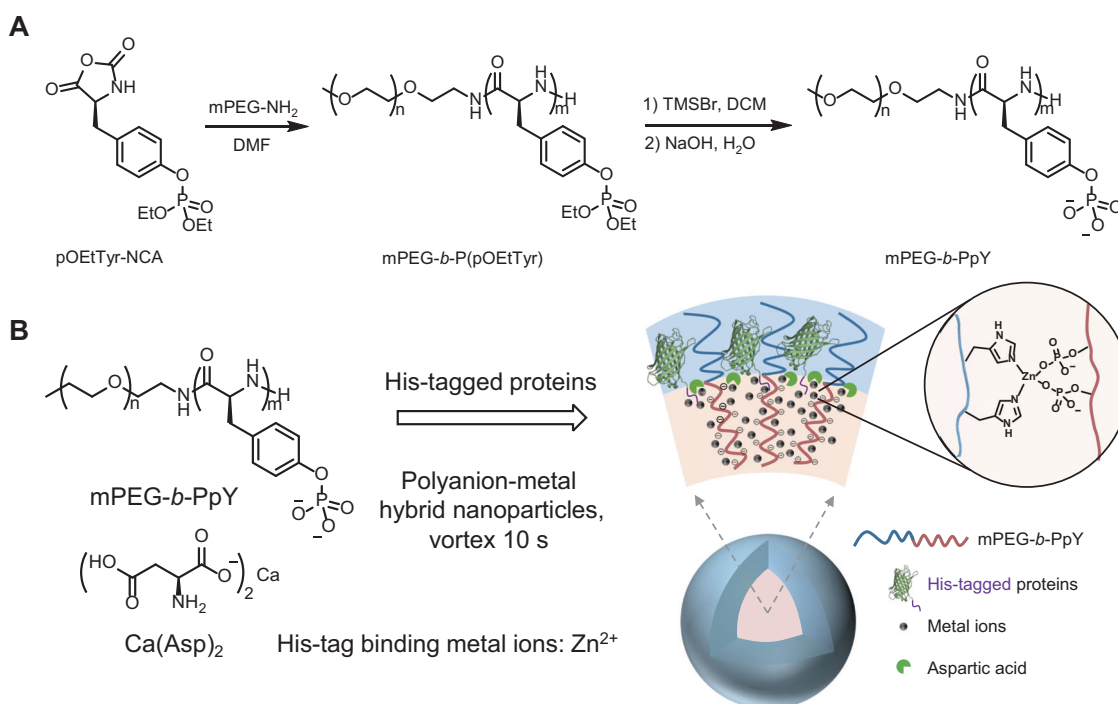


Fig. 1 **A** Synthesis of mPEG-*b*-PpY. **B** The ‘Mix and Go’ fabrication of mPEG-*b*-PpY-templated CaP nanoparticles for encapsulating and delivering His-tagged proteins

into delivery carriers, including nickel-immobilized polymers [28], metal–organic frameworks [29], and lipidoid nanoparticles [30]. Inspired by these pioneering works, we hypothesized that divalent metal ion-doped calcium phosphate (CaP) can be developed for the efficient delivery of His-tagged proteins, which has not been reported before. Naturally existing in many organisms and thanks to its attractive characteristics such as biocompatibility, biodegradability, and pH responsiveness [31], CaP has received wide attention as a biomedical material for dental restoration, bone repair, and tissue engineering [32]. More recently, CaP-based nanosystems have also been utilized to deliver small molecular drugs [33, 34], plasmid genes [35], and siRNAs [36, 37]. Herein, by doping His-tagged binding metal ions such as Zn²⁺ into a CaP-based nanocarrier, we successfully fabricated an intracellular delivery platform for His-tagged proteins (Fig. 1).

Results and discussion

Fabrication and characterization of the CaP-M nanoparticles

For drug delivery, preparing well-defined and stable nanocarriers less than 100 nm in diameter with narrow dispersity is critically important. Traditionally, CaP-based nanocarriers could be fabricated by the coassembly of a block copolymer

template and CaP microcrystals or by a two-step method consisting of self-assembly followed by hydrothermal treatment [31]. For instance, using poly(ethylene glycol)-*block*-poly(aspartic acid) (PEG-*b*-PAsp) as a PEGylated polyanion to prohibit the mineralization of large CaP blocks, Kataoka et al. prepared block copolymer-coated CaP nanoparticles for oligodeoxynucleotide and siRNA delivery [38].

In 2015, we first reported the synthesis of polyphosphotyrosine (PpY) by the ring-opening polymerization (ROP) of *N*-carboxyanhydride (NCA) [39]. Later, we established the block copolymer mPEG-*b*-PpY (Fig. 1A) as an effective carrier material for the delivery of cisplatin through phosphate-platinum coordination and Pt(IV)-based cationic polymeric prodrugs via electrostatic interactions [40–42]. Moreover, PpY exhibits acid-responsiveness and the ATP-triggered release of cisplatin [40]. Here, we hypothesized that mPEG-*b*-PpY could be used as a phosphate donor to interact with Ca²⁺ and generate CaP nanoparticles without an external phosphate source. The PEG segment was anticipated to stabilize the nanoparticle by forming a stealth outer layer. Moreover, we expected that the physicochemical properties of the nanoparticles could be readily tuned by doping with other metal ions (e.g., Zn²⁺, Mn²⁺, Ni²⁺, etc.) or small molecular chelating ligands such as amino acids.

First, we tested the formulation by simply mixing mPEG-*b*-PpY with CaCl₂ but failed to obtain stable nanoparticles under all conditions tested (data not shown). Therefore, we screened

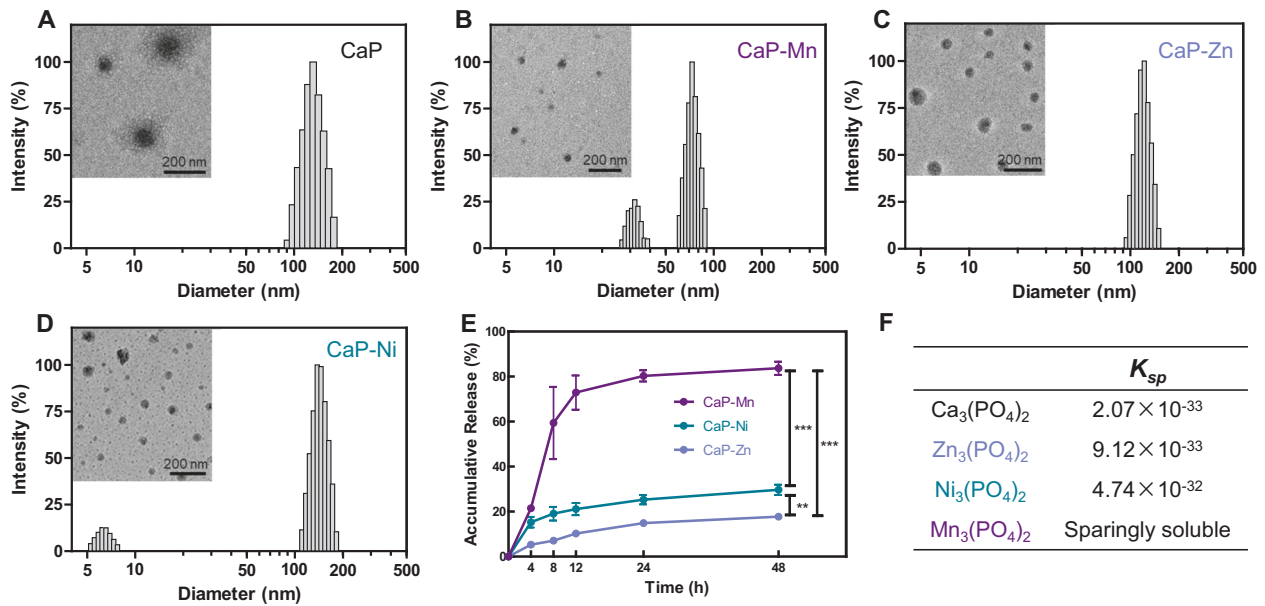


Fig. 2 Size and morphology of the CaP and CaP-M nanoparticles. Hydrodynamic sizes of CaP (A) with CaP-Mn (B), CaP-Zn (C), and CaP-Ni (D) as measured by DLS; inset photos are TEM images of the corresponding nanoparticles. Scale bar = 200 nm. E Release kinetics

of M^{2+} from CaP-M nanoparticles measured by ICP-MS. The p value was determined by two-way ANOVA: * $p < 0.05$, ** $p < 0.001$, *** $p < 0.0001$. F K_{sp} values of different $\text{M}_3(\text{PO}_4)_2$ (Data from CRC Handbook of Chemistry and Physics, 97th Edition)

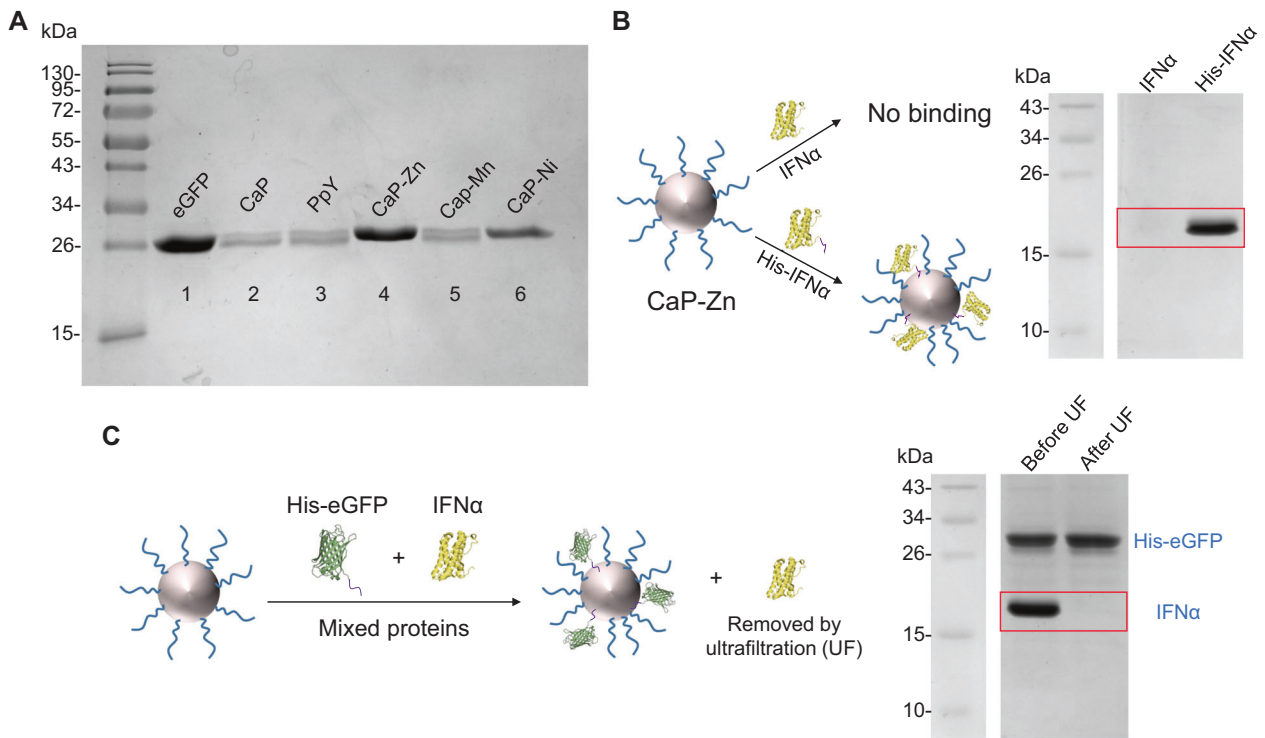


Fig. 3 A SDS-PAGE analysis of the His-eGFP contents of various nanoparticles. The corresponding nanoparticles or polymers were loaded with His-eGFP and purified with Ni-NTA affinity resins to remove unbound His-eGFP. B SDS-PAGE analysis of protein loading

in CaP-Zn incubated with IFN α or His-IFN α . C SDS-PAGE analysis of protein loading in CaP-Zn incubated with mixed IFN and His-eGFP. Protein@CaP-Zn was purified using ultrafiltration (UF) to remove the unbound protein (MWCO: 100,000 Da)

several anionic small molecular additives to stabilize the mPEG-*b*-PpY-templated CaP nanoparticle. We hypothesized that these additives may act as multivalent Ca^{2+} chelators that

compete with phosphate. Such an interplay could modulate the rate of CaP nucleation and eventually lead to stable hybrid CaP nanoparticles [43]. We found that aspartic acid, among all other

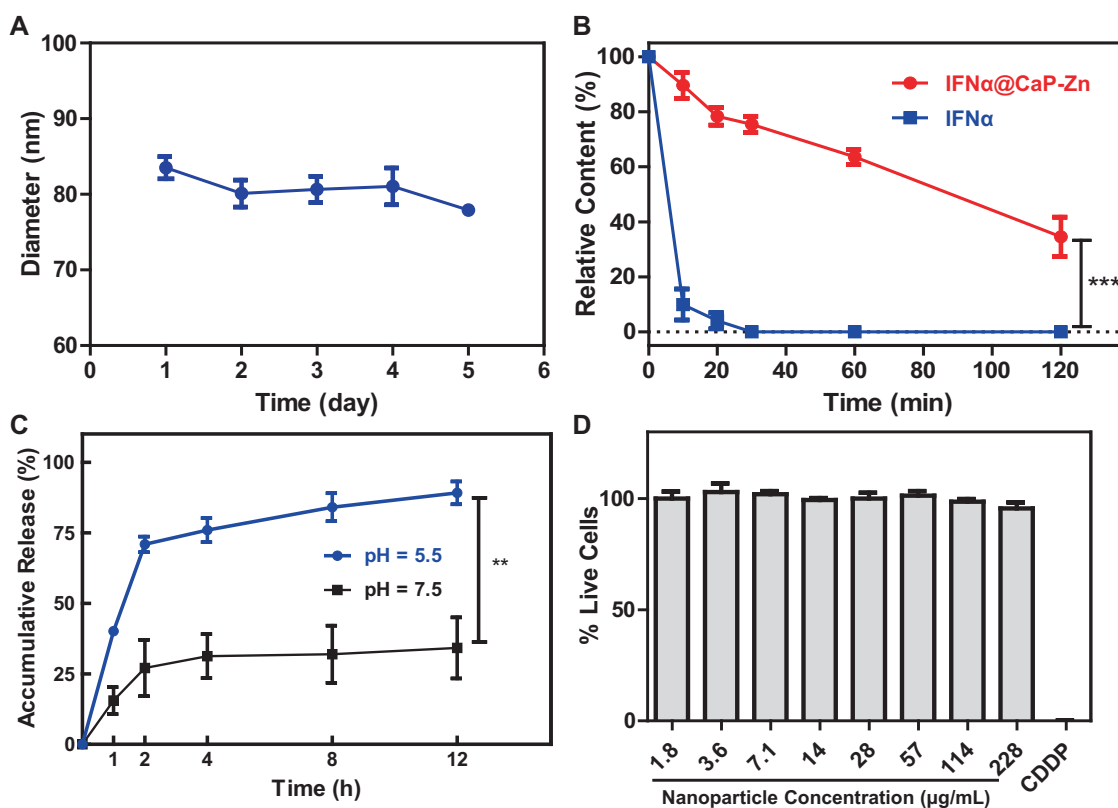


Fig. 4 **A** DLS determination of the diameters of the eGFP@CaP-Zn nanoparticles over time. Data are expressed as the means \pm SD from three independent experiments. **B** Chymotrypsin (30 μ g/mL)-mediated degradation of IFN α and IFN α @CaP-Zn. The experiments were repeated in triplicate, and error bars represent standard deviations. **C** Cumulative release of zinc ions (as measured by ICP-MS) from eGFP@CaP-Zn at pH 5.5 and 7.4. The *p* value was determined by

two-way ANOVA: **p* < 0.05, ***p* < 0.001, ****p* < 0.0001. **D** Viabilities of cells treated with eGFP@CaP-Zn nanoparticles at various concentrations. HeLa cells were incubated with eGFP@CaP-Zn at the denoted concentrations for 48 h before the cell viabilities were measured by CTB assay. Viabilities were normalized to the control group incubated with medium only, and data are shown as the means \pm SD; *n* = 3. CDDP was used as negative control

tested additives, was able to afford the most stable CaP nanoparticles with a controllable size and narrow size distribution (Table S1). To simplify the formation, calcium aspartate (Ca(Asp)₂) was selected to replace CaCl₂ and aspartic acid in future studies. The resulting nanoparticles were highly stable after purification, and the effective diameter barely changed after 7 days in HEPES saline buffer at room temperature (Fig. S2). For the 160 nm CaP nanoparticles in dynamic light scattering (DLS), transmission electron microscopy (TEM) revealed a similar diameter with a spherical morphology (Fig. 2A). To incorporate His-tag binding into the nanoparticles, different divalent metal ions ($M^{2+} = Zn^{2+}$, Mn^{2+} , Ni^{2+}) were doped into the system during the formulation of CaP. The changes in size and morphology of the metal ion-doped CaP (CaP-M) nanoparticles appeared to be minor except for CaP-Mn (Fig. 2B–D). Moreover, CaP-Mn displayed \sim 80% burst release of Mn^{2+} after 24 h of incubation in a dialysis bag [44], as shown in Fig. 2E, while CaP-Zn and CaP-Ni released only \sim 20% of the corresponding divalent metal ion under the same environment after 48 h. The difference in stability of CaP-M, as revealed from the M^{2+} release kinetics, might be a result

of the different solubility product constants (K_{sp} values) of the corresponding $M_3(PO_4)_2$ salts (Fig. 2F).

Incorporation of proteins to CaP-M nanoparticles

The mildly and biologically relevant conditions of the CaP-M formulation allowed us to add proteins to the nanoparticle solutions in situ. Briefly, CaP-M nanoparticle solutions were mixed with a model protein a His-tagged enhanced green fluorescent protein (His-eGFP), and incubated at 10 $^{\circ}$ C overnight. Unbound His-eGFP was removed by incubating the mixture with Ni-NTA affinity resins and collecting the supernatant. Sulfate polyacrylamide gel electrophoresis (SDS-PAGE) analysis of the purified His-eGFP@CaP-M showed almost no eGFP loading onto the CaP-M nanoparticles and other control groups, whereas considerable His-eGFP was found to be incorporated onto both the CaP-Zn and CaP-Ni nanoparticles (Fig. 3A). Notably, the loading of His-eGFP in CaP-Zn was almost 2 times that in CaP-Ni. The His-eGFP@CaP-M nanoparticles could also be purified using multiple rounds of

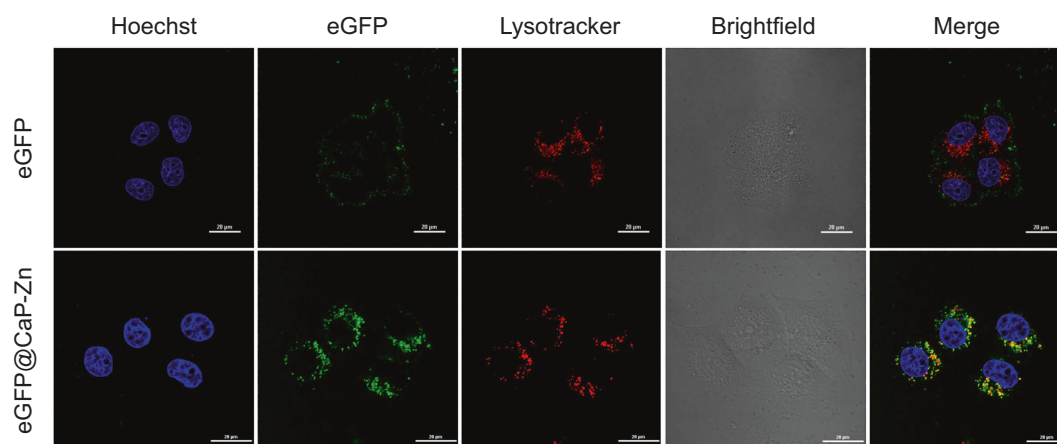


Fig. 5 Confocal laser scanning microscopy (CLSM) of the cellular uptake of His-eGFP or eGFP@CaP-Zn (50 $\mu\text{g}/\text{mL}$ in eGFP) in HeLa cells after 12 h of incubation. The nuclei and lysosomes were stained with Hoechst 33342 and LysoTracker Red, respectively. Scale bar = 20 μm

ultrafiltration (MWCO: 100,000 Da) in 50 mM HEPES saline buffer, which gave consistent protein loading results with those purified from the Ni-NTA resins. By measuring the fluorescence intensities and weights of the freeze-dried His-eGFP@CaP-Zn nanoparticles, the protein loading efficiency (PLE) and protein loading content (PLC) were calculated to be 53% and 32%, respectively. Considering the higher loading efficiency and the potential lower toxicity of zinc ions, we used CaP-Zn nanoparticles for further studies.

To verify that the proteins were attached to the CaP-Zn nanoparticles via the coordination bond of His-tag with Zn^{2+} , control studies were performed using proteins with or without a His-tag. First, we incubated interferon- α (IFN α) with or without a His-tag with CaP-Zn nanoparticles overnight. SDS-PAGE of the purified nanoparticles showed protein bands for only the nanoparticle incubated with IFN α bearing a His-tag but not for the group using IFN α without a His-tag (Fig. 3B). Next, His-eGFP and IFN α were mixed together and incubated with CaP-Zn. While the unpurified system displayed bands from both proteins, only His-eGFP was observed in the nanoparticles after ultrafiltration purification (Fig. 3C). Together, these results indicated that CaP-Zn nanoparticles can incorporate proteins in a His-tag-dependent manner.

To prepare CaP-Zn nanoparticles that are less than 100 nm in diameter, the relationship between particle size and metal ion concentration ratio was further studied (Table S2). It was found that with an increased proportion of Zn^{2+} , the size of the nanoparticles also gradually grew. After screening the concentrations of different components, CaP-Zn nanoparticles with an evenly distributed diameter of ~ 77 nm were obtained. The zeta potential of the CaP-Zn nanoparticles was 0.13 ± 0.42 mV after purification. After the loading of His-eGFP, the size of eGFP@CaP-Zn increased only slightly to ~ 80 nm. The stability of eGFP@CaP-Zn in

aqueous solution was monitored by DLS. As shown in Fig. 4A, the diameter of eGFP@CaP-Zn remained almost unchanged in HEPES saline buffer at room temperature for 5 days. Moreover, the color of eGFP in eGFP@CaP-Zn nanoparticles was almost completely preserved after 5 days, while the green color of free eGFP gradually faded away in aqueous solution at room temperature, suggesting that the protein loaded in eGFP@CaP-Zn would be more stable than if it was free floating in solution. To deliver proteins into cells, it is vital that the formulation protects the loaded protein from proteolytic degradation. For this, we incubated IFN α or IFN α @CaP-Zn with chymotrypsin at 37 $^{\circ}\text{C}$. As shown in Fig. 4B, IFN α alone was completely degraded after 30 min of chymotrypsin treatment. In contrast, $\sim 65\%$ IFN in IFN α @CaP-Zn remained intact after 1 h of incubation. Taken together, the protein was well protected after loading onto the CaP-Zn nanoparticles.

Intracellular delivery of protein@CaP-Zn

One attractive attribute of using CaP as the delivery vehicle is its pH-responsive degradation, which may lead to intracellular cargo release. To demonstrate the pH responsiveness of the nanoparticles, eGFP@CaP-Zn was dialyzed at pH 7.5 and 5.5, which imitated the pH of plasma and endosomes/lysosomes, respectively. The concentration of Zn^{2+} outside the dialysis bag was measured by ICP-MS over time. As shown in Fig. 4C, $\sim 75\%$ Zn^{2+} was released from the CaP-Zn nanoparticles within 2 h at pH 5.5, but the release rate of Zn^{2+} was much lower at pH 7.5. DLS analysis of the solution incubated at pH 5.5 also implied the degradation of the nanoparticles, as revealed by the significant drop in count rates. Viability assays indicated that Zn^{2+} was nontoxic at 369 μM (Fig. S3) and that the

eGFP@CaP-Zn nanoparticles were essentially nontoxic at concentrations up to 228 $\mu\text{g}/\text{mL}$ (Fig. 4D).

To investigate protein@CaP-Zn for intracellular delivery, we incubated the previously described eGFP@CaP-Zn or His-eGFP with HeLa cells in culture medium supplemented with 10% fetal bovine serum. We performed fluorescence staining of subcellular organelles using LysoTracker Red for lysosome localization and Hoechst 33342 for nuclei. As shown in Fig. 5, after 12 h of incubation, the control group cells showed almost no uptake of eGFP after washing with heparin sodium solution. The faint green fluorescence in the confocal laser scanning microscopy (CLSM) images came from the eGFP non-specifically absorbed onto the cell membrane. In contrast, for the eGFP@CaP-Zn group, the cells displayed bright green fluorescence in CLSM images. Although most of the nanoparticles were colocalized with lysosomes, indicating that the nanoparticles were taken up by cells through endocytosis, we also observed that a small portion of the green fluorescence escaped to the cytosol. These results demonstrated that the proteins loaded onto the CaP-Zn nanoparticles can be delivered to the intracellular space, but endosomal escape will need further optimization.

Conclusions

In summary, we developed a mPEG-*b*-PpY-templated CaP nanocarrier as a simple and general platform for the efficient loading and delivery of proteins. By fine-tuning the concentration of mPEG-*b*-PpY, divalent metal ion, and metal chelator aspartic acid, the final formulation yielded well-defined CaP nanoparticles that are less than 100 nm in diameter with narrow dispersity. This nanocarrier was generally applicable for binding His-tagged proteins via the coordination of oligohistidine with Zn^{2+} . Notably, this ‘Mix and Go’ strategy was mild and fully biocompatible, and the resulting protein@CaP-Zn nanoparticles could be directly used for downstream applications without further purification. Moreover, proteins loaded onto CaP-Zn nanoparticles can be protected from proteolytic degradation and effectively delivered to the intracellular spaces. Furthermore, the CaP-based nanocarrier was degradable in an acidic milieu, thus leading to intracellular cargo release. Overall, this work presented a novel CaP-based platform for protein delivery and may open up opportunities for protein-based theranostic applications.

Experimental section

Materials

All chemicals were purchased from commercial sources and used as received unless otherwise specified. Methoxypolyethylene

glycol amine (mPEG-NH₂, $M_w = 5000$ Da) was purchased from Aladdin Industrial Corporation (China). Zinc acetate dihydrate ($\text{Zn}(\text{Ac})_2 \cdot 2\text{H}_2\text{O}$), manganese(II) chloride tetrahydrate ($\text{MnCl}_2 \cdot 4\text{H}_2\text{O}$), and nickel sulfate hexahydrate ($\text{NiSO}_4 \cdot 6\text{H}_2\text{O}$) were purchased from Aladdin Industrial Corporation (China). L-Aspartic acid calcium salt ($\text{Ca}(\text{Asp})_2$) was purchased from Yuanye Bio-Technology (Shanghai, China). Anhydrous *N,N*-dimethylformamide (DMF) was purchased from Sigma-Aldrich. *O*-diethylphospho-L-tyrosine *N*-carboxyanhydride (pOEt-TyrNCA) was synthesized following previously reported procedures [39]. The proteins His-eGFP and His-IFN α were expressed by following reported protocols [45]. Wild-type IFN α (without the His-tag) was purchased from Sigma-Aldrich. *cis*-Diamminedichloroplatinum(II) (cisplatin, CDDP) was purchased from HWRK Chem Co., Ltd. (Beijing, China).

Instruments

NMR spectra were recorded on a 400 MHz Bruker ARX400 FT-NMR spectrometer. Inductively coupled plasma mass spectrometry (ICP-MS) was performed on a NexION 350X (PerkinElmer, U.S.A.). DLS and zeta potential measurements were conducted at 25 °C on a Nanobrook Omni (Brookhaven Instrument Corp. New York, U.S.A.), with a laser operating at 640 nm. Analyses were performed at an angle of 90° collecting optics. TEM was analyzed using a transmission electron microscope (JEM-2100F, Japan) at an accelerating voltage of 200 kV equipped with a field emission gun, an ultrahigh-resolution pole piece, and an ultrathin window JEOL detector. Images were obtained using an OSIS CANTEGA CCD camera. Confocal images were taken on a Nikon AIR confocal laser scanning microscope system attached to an inverted ECLIPSE Ti (Nikon Corp., Japan). The concentration of protein was measured with a NanoPhotometerTMP-class (Germany). SDS-PAGE analyses were recorded on a typhoon FLA 9500 laser scanner (GE Healthcare Corp.). Cytotoxicity studies were assayed with an EnSpire[®] Multimode Plate Reader (PerkinElmer, U.S.A.).

Synthesis of mPEG-*b*-PpY

PEG-*b*-PpY was synthesized according to a previous report [40]. In brief, the ROP of pOEt-TyrNCA was initiated by MeO-PEG-NH₂ ($M_w = 5000$ Da) in anhydrous DMF to obtain the block copolymer mPEG-*b*-P(pOEt-Tyr)₁₅. mPEG-P(pOEt-Tyr)₁₅ was characterized by ¹H NMR spectroscopy (Fig. S1A). To synthesize mPEG-*b*-PpY, bromotrimethylsilane (TMSBr) was added to mPEG-*b*-P(pOEt-Tyr)₁₅ in DCM. The mixture was continuously stirred at room temperature before it was concentrated under vacuum. The crude product was dissolved in sodium hydroxide

solution and dialyzed against 100 mM NaCl and subsequently ultrapure water. The resulting solution was lyophilized to afford mPEG-*b*-PpY as a white powder. The product was confirmed by ¹H NMR spectroscopy (Fig. S1B). The DP was determined by comparing the proton ratios of methylene units in PEG (–OCH₂CH₂–: δ = 3.7 ppm) and phenyl groups of PpY (–C₆H₄–: δ = 7.0 ppm) in ¹H-NMR spectra.

Fabrication and characterization of the mPEG-*b*-PpY-based CaP nanoparticles

CaP nanoparticles were fabricated according to the work of Peng Mi et al. in 2014 [46]. First, 50 μL of 100 mM Ca (Asp)₂ was diluted in 1 mL of 50 mM Tris-HCl buffer (pH 8) (solution A). mPEG-*b*-PpY at a concentration of phosphate group 1 mM was dissolved in 50 mM HEPES saline buffer (pH 7, NaCl 140 mM, without phosphate) (solution B). Solution B was quickly added to an equal volume of solution A with vigorous stirring with a vortex mixer for 10 s. The CaP nanoparticles were ultracentrifuged (MWCO: 100,000 Da) with 50 mM HEPES saline buffer. For the preparation of CaP nanoparticles doped with metal ions (CaP-M), stock solution A was obtained by adding salts containing corresponding metal ions, such as Zn(Ac)₂, MnCl₂, and NiSO₄, to Ca(Asp)₂ solution at an M²⁺/Ca²⁺ molar ratio of 1/5. The CaP-M nanoparticles were then prepared and purified according to the same protocol described above. The hydrodynamic sizes and size distributions of the CaP-M nanoparticles were evaluated by DLS and TEM. The zeta potential tests were performed in HEPES saline buffer (50 mM, pH 7). The release rates of metal ions from CaP nanoparticles were determined by inductively coupled plasma mass spectrometry (ICP-MS).

Fabrication of protein@CaP nanoparticles

The proteins with a His-tag (8 mg/mL × 75 μL) were added to CaP-M nanoparticle solutions ([pY] = 0.5 mM, 2 mL) and incubated in a 10 °C cold room for 12 h. To remove unbound proteins, the resulting protein@CaP-M nanoparticles were purified by two alternative routes: (1) ultrafiltration using 50 mM HEPES saline buffer or (2) incubation with Ni-NTA resin. Briefly, for route 2, an appropriate amount of Ni-NTA resin was added to the eGFP@CaP-X nanoparticle solution and gently agitated for 30 min at room temperature. The supernatants were then collected with a pipette. The size of the protein nanoparticles was monitored by DLS. Using His-eGFP as a model protein, the PLC and PLE were quantitatively determined by fluorescence analysis and sodium dodecyl

SDS-PAGE. ImageJ software was used to quantify the band intensity of SDS-PAGE. The PLC and PLE were calculated based on the following formulas:

$$\text{PLC (wt\%)} = (\text{weight of loaded protein/total weight of nanoparticles}) \times 100\%$$

$$\text{PLE (wt\%)} = (\text{weight of loaded protein/weight of feeding protein}) \times 100\%$$

Protease degradation assay

Briefly, in Tris-HCl buffer (50 mM pH 8), chymotrypsin (30 μg/mL, 0.1 equiv.) was incubated with IFNα or IFNα@CaP-Zn nanoparticles (final concentration: 0.3 mg/mL IFNα) at 37 °C. At each time point, an aliquot of the sample was removed and the reaction was terminated by boiling at 95 °C for 10 min. Samples at different time points were then analyzed by SDS-PAGE (Fig. S4). For quantitative analyses, IFNα was stained with Coomassie blue as determined by a typhoon scanner, followed by ImageJ analysis. All experiments were repeated in triplicate.

Cell viability assay

To determine the cytotoxicity of CaP-Zn nanoparticles, cells were seeded in a 96-well plate at a density of 5000 cells per well 24 h prior to treatment. The cells were incubated with CaP-Zn nanoparticles at a gradient of concentrations for 48 h (*n* = 3). Cell viabilities were determined by Cell-Titer-Blue Cell Viability Assay (Promega, U.S.A.). The assay was performed by following the manufacturers' procedures. IC50 values were obtained with GraphPad Prism version 5.

Release kinetics

Briefly, the metal-doped CaP-M nanoparticle solutions were placed into a dialysis bag (MWCO: 1000 Da) and incubated in 50 mM Tris-HCl buffer (pH 8, 99.0 mL) at room temperature. At each time point, 1.0 mL of solution outside the dialysis bag was removed and sampled for its metal (Zn²⁺, Ni²⁺, or Mn²⁺) concentration by ICP-MS. To keep the total volume unchanged outside the dialysis bag, 1.0 mL of Tris-HCl buffer was supplied back to the solution each time. The release kinetics of CaP-Zn at different pH values were measured by following a similar protocol. All experiments were repeated in triplicate.

Confocal laser scanning microscopy

HeLa cells (5 × 10⁴) in the exponential growth phase were seeded in cell culture dishes (20 mm, Nest), and the cells were incubated in Dulbecco's modified Eagle's medium

(DMEM; Corning, Manassas, U.S.A.) supplemented with 10% FBS (Gibco), 100 U/mL penicillin and 100 U/mL streptomycin (Corning, Manassas, U.S.A.) in a humidified atmosphere containing 5% CO₂ at 37 °C for 24 h. Then, 50 µg of protein (eGFP, eGFP@CaP-Zn) in 1 mL of fresh medium was added. After incubation for 12 h, the medium was removed, and the cells were washed with 1 mg/mL sodium heparin solution (1 mL × 3). The nuclei and lysosomes were then stained with Hoechst 33342 and Lyso-Tracker Red DND-99 (Life Technologies Inc. Carlsbad, U.S.A.), respectively, for 20 min at 37 °C in the dark. The stained cells were imaged in 1.0 mL of fresh medium after rinsing with PBS (1.0 mL × 3).

Acknowledgements This work was financially supported by the National Key Research and Development Program of China (No. 2016YFA0201400). We are thankful for the grant from the National Natural Science Foundation of China (21722401).

Compliance with ethical standards

Conflict of interest The authors declare no competing interests.

Publisher's note Springer Nature remains neutral with regard to jurisdictional claims in published maps and institutional affiliations.

References

1. Leader B, Baca QJ, Golan DE. Protein therapeutics: a summary and pharmacological classification. *Nat Rev Drug Discov.* 2008;7:21–39.
2. Urquhart L. Top companies and drugs by sales in 2020. *Nat Rev Drug Discov.* 2021;20:253.
3. Lv J, Fan Q, Wang H, Cheng Y. Polymers for cytosolic protein delivery. *Biomaterials.* 2019;218:119358.
4. Gu Z, Biswas A, Zhao M, Tang Y. Tailoring nanocarriers for intracellular protein delivery. *Chem Soc Rev.* 2011;40:3638–55.
5. Scaletti F, Hardie J, Lee YW, Luther DC, Ray M, Rotello VM. Protein delivery into cells using inorganic nanoparticle-protein supramolecular assemblies. *Chem Soc Rev.* 2018;47:3421–32.
6. Su S, Wang YY, Du FS, Lu H, Li ZC. Dynamic covalent bond-assisted programmed and traceless protein release: high loading nanogel for systemic and cytosolic delivery. *Adv Funct Mater.* 2018;28:1805287.
7. Wang R, Sheng K, Hou Y, Sun J, Lu H. Tailoring cationic helical polypeptides for efficient cytosolic protein delivery. *Chem Res Chin Univ.* 2020;36:134–8.
8. Li X, Wei Y, Wu Y, Yin L. Hypoxia-induced pro-protein therapy assisted by a self-catalyzed nanozymogen. *Angew Chem Int Ed.* 2020;59:22544–53.
9. He H, Chen Y, Li Y, Song Z, Zhong Y, Zhu R, et al. Effective and selective anti-cancer protein delivery via all-functions-in-one nanocarriers coupled with visible light-responsive, reversible protein engineering. *Adv Funct Mater.* 2018;28:1706710.
10. Yao P, Zhang Y, Meng H, Sun H, Zhong Z. Smart polymersomes dually functionalized with cRGD and fusogenic GALA peptides enable specific and high-efficiency cytosolic delivery of apoptotic proteins. *Biomacromolecules.* 2019;20:184–91.
11. Tong T, Wang L, You X, Wu J. Nano and microscale delivery platforms for enhanced oral peptide/protein bioavailability. *Biomater Sci.* 2020;8:5804–23.
12. Li Y, Bolinger J, Yu Y, Glass Z, Shi N, Yang L, et al. Intracellular delivery and biodistribution study of CRISPR/Cas9 ribonucleoprotein loaded bioreducible lipidoid nanoparticles. *Biomater Sci.* 2019;7:596–606.
13. Li Y, Jarvis R, Zhu K, Glass Z, Ogurlu R, Gao P, et al. Protein and mRNA delivery enabled by cholesteryl-based biodegradable lipidoid nanoparticles. *Angew Chem Int Ed.* 2020;59:14957–64.
14. Solaro R, Chiellini F, Battisti A. Targeted delivery of protein drugs by nanocarriers. *Materials.* 2010;3:1928–80.
15. Zhou HX, Pang X. Electrostatic interactions in protein structure, folding, binding, and condensation. *Chem Rev.* 2018;118:1691–741.
16. Dutta K, Kanjilal P, Das R, Thayumanavan S. Synergistic interplay of covalent and non-covalent interactions in reactive polymer nanoassembly facilitates intracellular delivery of antibodies. *Angew Chem Int Ed.* 2021;60:1821–30.
17. Ekladios I, Colson YL, Grinstaff MW. Polymer-drug conjugate therapeutics: advances, insights and prospects. *Nat Rev Drug Discov.* 2019;18:273–94.
18. Wang H, Hou Y, Hu Y, Dou J, Shen Y, Wang Y, et al. Enzyme-activatable interferon-poly(α -amino acid) conjugates for tumor microenvironment potentiation. *Biomacromolecules.* 2019;20:3000–8.
19. Shen BQ, Xu K, Liu L, Raab H, Bhakta S, Kenrick M, et al. Conjugation site modulates the in vivo stability and therapeutic activity of antibody-drug conjugates. *Nat Biotechnol.* 2012;30:184–9.
20. Honda Y, Nomoto T, Matsui M, Takemoto H, Kaihara Y, Miura Y, et al. Sequential self-assembly using tannic acid and phenylboronic acid-modified copolymers for potential protein delivery. *Biomacromolecules.* 2020;21:3826–35.
21. Lv J, Wang C, Li H, Li Z, Fan Q, Zhang Y, et al. Bifunctional and bioreducible dendrimer bearing a fluoroalkyl tail for efficient protein delivery both in vitro and in vivo. *Nano Lett.* 2020;20:8600–7.
22. Ren L, Lv J, Wang H, Cheng Y. A coordinative dendrimer achieves excellent efficiency in cytosolic protein and peptide delivery. *Angew Chem Int Ed.* 2020;59:4711–9.
23. Zhang S, Cheng Y. Boronic acid-engineered gold nanoparticles for cytosolic protein delivery. *Biomater Sci.* 2020;8:3741–50.
24. Liu J, Luo T, Xue Y, Mao L, Stang PJ, Wang M. Hierarchical self-assembly of discrete metal-organic cages into supramolecular nanoparticles for intracellular protein delivery. *Angew Chem Int Ed.* 2021;60:5429–35.
25. Yang X, Tang Q, Jiang Y, Zhang M, Wang M, Mao L. Nanoscale ATP-responsive zeolitic imidazole framework-90 as a general platform for cytosolic protein delivery and genome editing. *J Am Chem Soc.* 2019;141:3782–6.
26. Hochuli E, Bannwarth W, Döbeli H, Gentz R, Stüber D. Genetic approach to facilitate purification of recombinant proteins with a novel metal chelate adsorbent. *Nat Biotechnol.* 1988;6:1321–5.
27. Porath J. Immobilized metal ion affinity chromatography. *Protein Expr Purif.* 1992;3:263–81.
28. Postupalenko V, Desplancq D, Orlov I, Arntz Y, Spohner D, Mely Y, et al. Protein delivery system containing a nickel-immobilized polymer for multimerization of affinity-purified His-tagged proteins enhances cytosolic transfer. *Angew Chem Int Ed.* 2015;54:10583–6.
29. Roder R, Preiss T, Hirschle P, Steinborn B, Zimpel A, Hohn M, et al. Multifunctional nanoparticles by coordinative self-assembly of His-tagged units with metal-organic frameworks. *J Am Chem Soc.* 2017;139:2359–68.
30. Li Y, Li AC, Xu Q. Intracellular delivery of His-tagged genome-editing proteins enabled by nitrilotriacetic acid-containing lipidoid nanoparticles. *Adv Healthc Mater.* 2019;8:e1800996.
31. Huang D, He B, Mi P. Calcium phosphate nanocarriers for drug delivery to tumors: imaging, therapy and theranostics. *Biomater Sci.* 2019;7:3942–60.
32. LeGeros RZ. Biodegradation and bioresorption of calcium phosphate ceramics. *Clin Mater.* 1993;14:65–88.

33. Shi H, Cheng Q, Yuan S, Ding X, Liu Y. Human serum albumin conjugated nanoparticles for pH and redox-responsive delivery of a prodrug of cisplatin. *Chemistry*. 2015;21:16547–54.
34. Nomoto T, Fukushima S, Kumagai M, Miyazaki K, Inoue A, Mi P, et al. Calcium phosphate-based organic-inorganic hybrid nanocarriers with pH-responsive on/off switch for photodynamic therapy. *Biomater Sci*. 2016;4:826–38.
35. Kakizawa Y, Miyata K, Furukawa S, Kataoka K. Size-controlled formation of a calcium phosphate-based organic–inorganic hybrid vector for gene delivery using poly(ethylene glycol)-block-poly (aspartic acid). *Adv Mater*. 2004;16:699–702.
36. Choi KY, Silvestre OF, Huang X, Min KH, Howard GP, Hida N, et al. Versatile RNA interference nanoplatfor for systemic delivery of RNAs. *ACS Nano*. 2014;8:4559–70.
37. Pittella F, Cabral H, Maeda Y, Mi P, Watanabe S, Takemoto H, et al. Systemic siRNA delivery to a spontaneous pancreatic tumor model in transgenic mice by PEGylated calcium phosphate hybrid micelles. *J Control Release*. 2014;178:18–24.
38. Kakizawa Y, Furukawa S, Kataoka K. Block copolymer-coated calcium phosphate nanoparticles sensing intracellular environment for oligodeoxynucleotide and siRNA delivery. *J Control Release*. 2004;97:345–56.
39. Sun Y, Hou Y, Zhou X, Yuan J, Wang J, Lu H. Controlled synthesis and enzyme-induced hydrogelation of poly(l-phosphotyrosine)s via ring-opening polymerization of α -amino acid N-carboxyanhydride. *ACS Macro Lett*. 2015;4:1000–3.
40. Hou Y, Wang Y, Wang R, Bao W, Xi X, Sun Y, et al. Harnessing phosphato-platinum bonding induced supramolecular assembly for systemic cisplatin delivery. *ACS Appl Mater Interfaces*. 2017;9:17757–68.
41. Li SL, Hou Y, Hu Y, Yu J, Wei W, Lu H. Phosphatase-triggered cell-selective release of a Pt(iv)-backboned prodrug-like polymer for an improved therapeutic index. *Biomater Sci*. 2017;5:1558–66.
42. Li SL, Wang Y, Zhang J, Wei W, Lu H. Targeted delivery of a guanidine-pendant Pt(iv)-backboned poly-prodrug by an anisamide-functionalized polypeptide. *J Mater Chem B*. 2017;5:9546–57.
43. Kohri K, Umekawa T, Kodama M, Katayama Y, Ishikawa Y, Takada M, et al. Inhibitory effect of glutamic acid and aspartic acid on calcium oxalate crystal formation. *Eur Urol*. 1990;17:173–7.
44. Mi P, Kokuryo D, Cabral H, Wu H, Terada Y, Saga T, et al. A pH-activatable nanoparticle with signal-amplification capabilities for non-invasive imaging of tumour malignancy. *Nat Nanotechnol*. 2016;11:724–30.
45. Hou Y, Yuan J, Zhou Y, Yu J, Lu H, Concise A. Approach to site-specific topological protein-poly(amino acid) conjugates enabled by in situ-generated functionalities. *J Am Chem Soc*. 2016;138:10995–11000.
46. Mi P, Kokuryo D, Cabral H, Kumagai M, Nomoto T, Aoki I, et al. Hydrothermally synthesized PEGylated calcium phosphate nanoparticles incorporating Gd-DTPA for contrast enhanced MRI diagnosis of solid tumors. *J Control Release*. 2014;174:63–71.